Impact of Isotopic Exchange on Hydrated Protein Dynamics Revealed by Polarized Neutron Scattering

Agathe Nidriche,[1,2] Martine Moulin,[2] Philippe Oger,[3] J. Ross Stewart,[4] Lucile Mangin-Thro,[2] Wolfgang Schmidt,[5] Gerald Kneller,[6,7] and Judith Peters[1,2,8,*]

[1]*Université Grenoble Alpes, CNRS, LiPhy, 38400 Grenoble, France*
[2]*Institut Laue Langevin, 38042 Grenoble, France*
[3]*Université de Lyon, UCBL, INSA Lyon, CNRS, MAP UMR 5240, 69621 Villeurbanne, France*
[4]*ISIS Neutron and Muon Source, Rutherford Appleton Laboratory, Didcot OX11 0QX, United Kingdom*
[5]*Jülich Centre for Neutron Science (JCNS), Forschungszentrum Jülich GmbH, Outstation at ILL, Boîte Postale 156, 38042 Grenoble, France*
[6]*Centre de Biophysique Moléculaire, CNRS and Université d'Orléans, Rue Charles Sadron, 45071 Orléans, France*
[7]*Synchrotron Soleil, L'Orme de Merisiers, 91192 Gif-sur-Yvette, France*
[8]*Institut Universitaire de France, 75231 Paris, France*

(Received 18 September 2023; accepted 22 December 2023; published 25 January 2024)

Within the last decades, it was often assumed that in hydrogen-rich disordered samples, such as proteins in solution or hydrated powder form, incoherent neutron scattering from hydrogen nuclei dominated the scattering signal to an extent that allowed all other contributions to be neglected. As incoherent scattering arises solely from self-correlations, it further justified such a choice. Consequently, heavy water was often used as a contrast tool to highlight molecular motions in live samples. Coherent scattering, which implies the scattering from many nuclei and therefore collective processes, is another non-negligible contribution to neutron scattering where cross sections of other nuclei than hydrogen are significant. The recent advent of instrumentation based on polarization of neutron beams and the analysis of their polarization state after scattering for dynamical studies allows us to separate and shed light on the two contributions. In the present study we reveal that, unexpectedly, the isotopic exchange of water in the hydration shell of proteins arises on a much faster timescale than assumed so far. Moreover, the collective and local D-bond network relaxation of hydration water contributes to a high extent to the coherent scattering signal, at odds with usual "static" approaches used to estimate the relative impacts of dynamics in the sample. Hence, hydration water necessarily contaminates nonpolarized standard experiments. The findings are of paramount importance for all neutron scattering experiments where partial or full deuteration is used.

DOI: 10.1103/PRXLife.2.013005

I. INTRODUCTION

It is inherent to neutron scattering that the measured signal contains both an incoherent and a coherent contribution [1]. Incoherent scattering yields information on single-atom averaged motions and therefore sheds light on molecular dynamics, whereas coherent scattering provides information on structure and collective motions. The coherent contribution contains two terms: one arising from the scattering of single nuclei, holding the same information as incoherent scattering and denoted the "self" term, and one implying scattering from pairs of distinct nuclei (interferences), such as between two distinct hydrogen atoms or between a carbon and a nitrogen atom in the sample. The latter is denoted "distinct" and therefore corresponds to a collective process. As hydrogen has the highest incoherent neutron scattering cross section among all atoms contained in life science molecules (about 40 times that of all others), it is assumed that the contribution from other atoms can be neglected [2]. Therefore, quasielastic neutron scattering (QENS) is usually the preferred technique to investigate the diffusive dynamics of hydrogen-rich samples from the picosecond to the nanosecond timescale, such as biological molecules, which contain a majority of equally spread H atoms (typically around 50%). The situation is more complex for coherent scattering, where several atoms contribute more or less equally to the total coherent scattering cross section.

Neutron scattering is moreover sensitive to isotope exchange; i.e., it differs when a neutron scatters from hydrogen or deuterium. This can be advantageously used when one wants to highlight specific parts of the sample, for instance, to enhance the protein's self-dynamics compared to the surrounding water. This is known as H/D contrast matching [3]. Another typical interest is the investigation of hydration water dynamics at the protein's surface when using a perdeuterated protein hydrated in H_2O [4–6]. Moreover, perdeuteration has also been proposed as a possibility to investigate internal collective motions of proteins in D_2O [7–9].

However, the studies demonstrating the effectiveness of such a deuteration procedure to hide or separate contribu-

*Corresponding author: jpeters@ill.fr

Published by the American Physical Society under the terms of the Creative Commons Attribution 4.0 International license. Further distribution of this work must maintain attribution to the author(s) and the published article's title, journal citation, and DOI.

tions in QENS are scarce. This is now made possible with the advent of high-flux time-of-flight neutron spectrometers equipped with polarization analysis [10] to separate exactly incoherent and coherent contributions [11] from the analysis of the neutron's spin state at the detectors, with good energy resolution. This had long remained a challenge due to strong flux reduction and technical impediments [12]. Moreover, QENS probes large ranges of momentum transfer Q. In hydrated or solubilized proteins, for Q values below $Q = 0.4$ Å^{-1} which are equivalent to distances $r = 2\pi/Q$ in the range of intermolecular distances (SANS region), coherent scattering can largely dominate. It was unambiguously shown with polarized diffraction by Gaspar *et al.* [13] on protonated myoglobin and deuterated C-phycocyanin. On the other hand, at larger Q values, incoherent scattering dominates despite the impact of the Debye-Waller factor, while structural information remains non-negligible especially around the main peak corresponding to near-neighbor distances ($Q \approx 1.5$–2 Å^{-1}). Hence, a strict separation of coherent and incoherent scattering requires polarization analysis in hydrated proteins.

Up to now, the few studies that have explored coherent QENS with a polarized beam have highlighted the nontriviality of structural relaxation as a function of momentum transfer and time in D_2O and van der Waals liquids [14–16], or reported underestimation of incoherent diffusion coefficients in the case of ionic liquids in nonpolarized experiments [17,18].

Therefore, we question in this study what happens when a perdeuterated protein is measured in D_2O, where sample and hydration water equally contribute to coherent scattering. We also challenge the assumption that a protonated protein should dominate the signal when surrounded by heavy hydration water. Generally speaking, we dispute the use of the "static picture" offered by the comparison of atomic cross sections in the sample to deduce which parts of the sample are invisible or emphasized, especially in dynamical studies of biomolecules, where relaxation timescales are broad and heterogeneous.

II. METHODS

We use the green fluorescent protein (GFP) as a model system for our study, both in protonated (pGFP) and perdeuterated (dGFP) hydrated powder forms, studied at the physiological temperature $T = 310$ K. A hydration of $h = 0.4$ ($h =$ g D_2O/g protein) is standard to ensure the onset of side-chain motions, covering at least a whole hydration layer [19]. The sample production is detailed in the Supplemental Material (SM) [20] (see also Refs. [3,21,22] therein). We used the same hydration protocol for the three experiments. We first performed polarized diffraction experiments on the D7 diffuse diffractometer [12] and on the IN12 triple-axis spectrometer (TAS) [23] at Institut Laue-Langevin, France (ILL). We then proceeded with experiments on the LET time-of-flight (TOF) spectrometer equipped with polarization analysis at the ISIS Neutron and Muon Source, UK, with resolution $\Delta E \approx 95$ μeV [10,24,25]. Experiments and instruments are described in the SM, Table S1 and Sec. II A.

Once data reduction was carried out [26–29], data analysis was performed according to the approach described in Refs. [30–32], where Ref. [32] contains also a link to the corresponding deposited codes. The concept of our analysis and the model are briefly outlined below.

The basic quantity obtained from neutron scattering experiments is the dynamic structure factor,

$$S(\mathbf{Q},\omega) = \frac{1}{2\pi}\int_{-\infty}^{+\infty} dt\ \exp(i\omega t) F(\mathbf{Q},t), \tag{1}$$

where $\mathbf{Q}$ and ω are, respectively, the momentum and energy transfer from the neutron to the scattering atom in units of $\hbar$ and $F(\mathbf{Q},t)$ is referred to as an intermediate scattering function,

$$F(\mathbf{Q},t) = \frac{1}{N}\sum_{j,k}\Gamma_{jk}\langle e^{-i\mathbf{Q}\cdot\hat{\mathbf{r}}_j(0)} e^{i\mathbf{Q}\cdot\hat{\mathbf{r}}_k(t)}\rangle. \tag{2}$$

Here N is the number of atoms in the sample, $\langle\cdots\rangle$ denotes a quantum ensemble average, and $\hat{\mathbf{r}}_j(t)$ is the position operator of atom j in the Heisenberg picture. The weights Γ_{jk} are given by

$$\Gamma_{jk} = b^*_{j,\mathrm{coh}} b_{k,\mathrm{coh}} + \delta_{jk}|b_{j,\mathrm{inc}}|^2, \tag{3}$$

where $b_{j,\mathrm{coh}}$ is the coherent and $b_{j,\mathrm{inc}}$ the incoherent scattering length of atom j. The intermediate scattering function splits thus into a coherent part, reflecting the structural dynamics of the atoms in the scattering system, and an incoherent part resulting from single-atom contributions. It implies that

$$F(\mathbf{Q},t) = F_{\mathrm{coh}}(\mathbf{Q},t) + F_{\mathrm{inc}}(\mathbf{Q},t). \tag{4}$$

We normalize the weighting factors such that

$$\lim_{Q\to\infty} F(\mathbf{Q},0) = \frac{1}{N}\sum_j \Gamma_{jj} = 1. \tag{5}$$

Defining the dynamical variable

$$\delta\hat{\rho}_j(\mathbf{Q},t) \equiv e^{i\mathbf{Q}\cdot\hat{\mathbf{r}}_j(t)} - \langle e^{i\mathbf{Q}\cdot\hat{\mathbf{r}}_j}\rangle, \tag{6}$$

the intermediate scattering function can be written in the generic form

$$F(\mathbf{Q},t) = F(\mathbf{Q},\infty) + (F(\mathbf{Q},0) - F(\mathbf{Q},\infty))\phi(\mathbf{Q},t), \tag{7}$$

emphasizing its relaxation towards a $\mathbf{Q}$-dependent plateau value, $F(\mathbf{Q},\infty) \equiv ESF(\mathbf{Q})$, where ESF is the elastic scattering factor. The corresponding initial value, $F(\mathbf{Q},0)$, is the static structure factor,

$$F(\mathbf{Q},0) = \int_{-\infty}^{+\infty} d\omega\, S(\mathbf{Q},\omega) \equiv S(\mathbf{Q}), \tag{8}$$

and the relaxation function $\phi(\mathbf{Q},t)$ can be expressed as

$$\phi(\mathbf{Q},t) = \frac{\sum_{j,k}\Gamma_{jk}\langle\delta\hat{\rho}_j(\mathbf{Q},0)^\dagger\delta\hat{\rho}_k(\mathbf{Q},t)\rangle}{\sum_{j,k}\Gamma_{jk}\langle\delta\hat{\rho}_j(\mathbf{Q},0)^\dagger\delta\hat{\rho}_k(\mathbf{Q},0)\rangle}. \tag{9}$$

For essentially incoherent scattering from hydrogen-rich samples, we have $F(\mathbf{Q},0) = 1$, the limit $F(\mathbf{Q},\infty)$ corresponds to the elastic incoherent scattering factor EISF($\mathbf{Q}$), and the relaxation function, $\phi(\mathbf{Q},t)$, contains only self-contributions ($j = k$) from the predominantly scattering hydrogen atoms.

The data analysis is performed for the resolution-deconvolved intermediate scattering function, using the generic form given in Eq. (7). We use a semiclassical approximation of the intermediate scattering function [33]

$$F_{\mathrm{cl}}(\mathbf{Q},t) \approx \frac{F(\mathbf{Q},t + i\beta\hbar/2)}{F(\mathbf{Q},i\beta\hbar/2)}, \tag{10}$$

identifying the symmetrized and correctly normalized quantum correlation function with the classical counterpart, which has the same symmetry properties. We note here that in the quantum case $F^*(\mathbf{Q},t) = F(\mathbf{Q},-t)$ and $F(\mathbf{Q},t) = F(-\mathbf{Q},-t+i\beta\hbar)$.

Our "minimalist" few-parameter model has been used in previous publications for proteins [30–32] and water [34] and it has its roots in a quantum energy landscape approach to neutron scattering from complex systems combined with asymptotic analysis [35]. Power-law relaxation, which is typical for proteins and complex systems in general [36–39], is in particular accounted for and in the framework of classical statistical mechanics it can be motivated by fractional kinetics in complex energy landscapes [40–42], as well as by long-time memory effects created by the interaction of a large number of interacting particles, which are described in the framework of the generalized Langevin equation [43,44]. The relaxation function appearing in Eq. (7), which is here considered in the classical limit, is modeled by a stretched Mittag-Leffler function (the $\mathbf{Q}$ dependence is omitted)

$$\phi_{\rm cl}(t) = E_\alpha(-(|t|/\tau)^\alpha), \quad 0 < \alpha \leqslant 1, \tag{11}$$

$E_\alpha(\cdot)$ denotes the Mittag-Leffler (ML) function [45,46] and $\alpha \equiv \alpha(\mathbf{Q})$ and $\tau \equiv \tau(\mathbf{Q})$ are $\mathbf{Q}$-dependent form and scale parameters, respectively. The ML function is defined by the series

$$E_\alpha(z) = \sum_{k=0}^{\infty} \frac{z^k}{\Gamma(1+\alpha k)}, \tag{12}$$

with $z \in \mathbb{C}$ and $\alpha \in \mathbb{C}$. Since $E_1(z) = \exp(z)$, it can thus be considered a generalized exponential function. For $0 < \alpha < 1$ the model relaxation function decays monotonously and asymptotically with a power law,

$$\phi_{\rm cl}(t) \overset{t\to\infty}{\sim} \frac{(t/\tau)^{-\alpha}}{\Gamma(1-\alpha)}. \tag{13}$$

For $\alpha = 1$, i.e., for exponential decay, the power-law long-time tail vanishes on account of $\lim_{z\to 0}\Gamma(z) = \infty$. Referring to the asymptotic form of the intermediate scattering function given in Eq. (7), our model has three parameters: (1) the timescale parameter $\tau \equiv \tau(\mathbf{Q})$, (2) the form parameter $\alpha \equiv \alpha(\mathbf{Q})$, and (3) the elastic intensity $F(\mathbf{Q},\infty)$. The form parameter α integrates nonexponential relaxation of individual hydrogen atoms as well as motional heterogeneity of different atoms.

The separation of $S_{\rm coh}(\mathbf{Q},\omega)$ and $S_{\rm inc}(\mathbf{Q},\omega)$ in the TOF experiment is a linear combination of the spin-flip (sf, $\uparrow\downarrow$ or $\downarrow\uparrow$) and non-spin-flip (nsf, $\uparrow\uparrow$ or $\downarrow\downarrow$) intensities of the polarized incoming beam upon scattering (see Fig. 1). The method is further described in Sec. II B of the SM [20] (see Refs. [47,48]).

In our case, scattering functions depend only on $Q = |\mathbf{Q}|$ due to the isotropy of the powder sample:

$$\begin{aligned} S_{\rm coh}(Q,\omega) &= S^{\rm nsf}(Q,\omega) - \tfrac{1}{2}S^{\rm sf}(Q,\omega), \\ S_{\rm inc}(Q,\omega) &= \tfrac{3}{2}S^{\rm sf}(Q,\omega). \end{aligned} \tag{14}$$

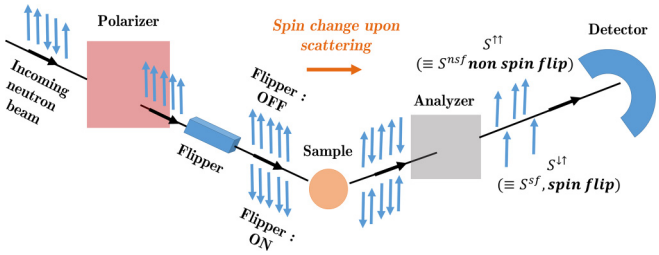

FIG. 1. Schematics of uniaxial polarization analysis performed for neutron spectroscopy or diffraction. It consists in polarizing the neutron beam ahead of the sample, and analyzing it after scattering. Flipping the spin makes it possible to get the differential cross sections in the spin-flip and non-spin-flip cases.

III. D_2O HYDRATION WATER LAYER ISOTOPIC EXCHANGE PROBED WITH NEUTRON POLARIZED DIFFRACTION

Neutron polarization analysis gives us the means to verify common assumptions in neutron scattering applied to life sciences, one of them being the predominance of coherent scattering in a deuterated biomolecule hydrated in D_2O. This assumption underlies many studies carried out since perdeuteration of whole molecules has become possible, either to highlight water dynamics when hydrated in H_2O [4–6] or to provide information on the protein collective dynamics when hydrated in D_2O [7–9]. In the latter case corresponding to our sample preparation, it also presumes a perfect isotopic state of the sample, where exchanges are minor during sample production, preparation, or data acquisition. To decipher whether incoherent or coherent scattering prevails in dGFP powder hydrated with D_2O, a first indicator is provided by the ratio of coherent over total static structure factors, $S_{\rm coh}(Q)/S_{\rm tot}(Q)$, obtained with polarized neutron diffraction, where $S(Q)$ is expressed in Eq. (8). In the large-Q limit (Sec. III A of the SM [20]), this ratio is expected to obey

$$\lim_{Q\to\infty} \frac{S_{\rm coh}(Q)}{S_{\rm tot}(Q)} = \frac{\sigma_{\rm coh,self}}{\sigma_{\rm coh,self} + \sigma_{\rm inc,self}}, \tag{15}$$

where $\sigma_{\rm self} = \sum_i N_i b_i^2/4\pi$ is the self-bound cross section of the nucleus tabulated in Ref. [2], with i the nucleus type and N_i the number of nuclei of type i. Therefore, we asymptotically expect a ratio of 83%, indicating strong impact of coherent scattering and, hence, non-negligible collective dynamics in the sample.

Experimental ratios were evaluated at physiological temperature with IN12, D7, and LET instruments and are represented in Fig. 2 by blue, orange, and green dots, respectively. These are almost identical within error bars despite small variability in sample preparation and despite different dynamical ranges of the three instruments (see Table S1 of the SM [20]).

We found out that the mean experimental value for $S_{\rm coh}(Q)/S_{\rm tot}(Q)$ averaged on $Q \in [0.5, 2]$ Å^{-1} was close to 25% (Table I), at odds with Eq. (15) and the hypothesis of prevalence of coherent scattering. The highest peak around $Q = 1.4$ Å^{-1}, which mainly corresponds to C-C correlations, exhibits a ratio of only ≈30%. This low ratio cannot be explained only by the well-documented isotopic exchange of

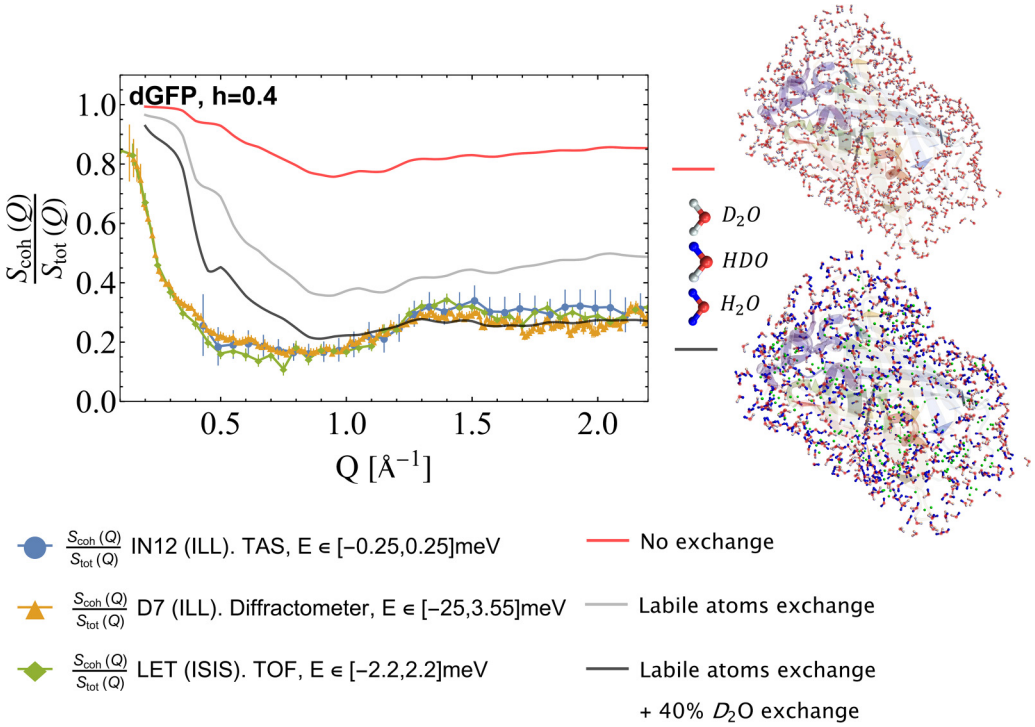

FIG. 2. dGFP sample, $h = 0.4$ at $T = 310$ K. The experimental ratio of coherent over total static structure factors, $S_{coh}(Q)/S_{tot}(Q)$, was measured on the D7 diffuse diffractometer, ILL (orange △), the IN12 triple-axis spectrometer, ILL (blue ○), and the LET TOF, ISIS (green ◇) with different dynamical ranges (legend; see Table S1 of the SM [20] for further information). Experimental ratios are compared to the ratios calculated from all distances in the protein and its hydration water, using 6l26.PDB. These are calculated in the case where the whole hydration layer is deuterated (red line), in the case of labile atoms exchange in the protein (414 hydrogens in total, gray line), and in the case of labile atoms exchange in the protein + 40% D → H exchange in the hydration water of GFP (black line). On the right-hand side, we display two sketches of the protein surrounded by its hydration water. The top one corresponds to the calculated red line: no exchange in GFP's hydration water. At the bottom, it corresponds to the black line: labile atoms (in green) and 40% of hydration water (hydrogen atoms in blue) have exchanged.

all labile deuterium atoms bonded to O, S, and N atoms in the presence of hydrogen [49]: in that case, one asymptotically gets $S_{coh}(Q)/S_{tot}(Q) = 41\%$ (Table I). Last but not least, $S_{coh}(Q)/S_{tot}(Q)$ remains the same within error bars at $T = 2$ K and $T = 310$ K on LET (see Fig. S7 of the SM [20]), hence highlighting the robustness of the high incoherent contribution in this Q range and excluding that it arises from an inelastic effect at physiological temperature. We assume that discrepancies between assumptions and our experiments do not arise because our Q range is restricted to 2 Å^{-1}: deuterated protein powder diffraction reports that the main peak's scattering intensity at $Q = 1.4$ Å^{-1} is higher than for the large-Q limit [50].

TABLE I. Comparison of the cross-section ratio $\frac{\sigma_{coh,self}}{\sigma_{tot,self}}$ to the experimental ratio $\frac{S_{coh}(Q)}{S_{tot}(Q)}$ for pGFP and dGFP.

Sample	$\left(\frac{\sigma_{coh,self}}{\sigma_{coh,self}+\sigma_{inc}}\right)$	$\left(\frac{\sigma_{coh,self}}{\sigma_{coh,self}+\sigma_{inc}}\right)$[a] lab. exch.	$\left(\frac{S_{coh}(Q)}{S_{tot}(Q)}\right)$[b] exp
$dGFP_{h=0.4}$[c]	0.83	0.41	0.25
$pGFP_{h=0.4}$[d]	0.16	0.13	0.15

[a]All labile atoms have exchanged in the protein, 414 atoms.
[b]Average of experimental ratios, LET, IN12, D7, $T = 310$ K.
[c]$D_{1919}C_{1261}N_{342}O_{379}S_8 + D_{1202}O_{601}$.
[d]$H_{1919}C_{1261}N_{342}O_{379}S_8 + D_{1126}O_{563}$.

In order to explain such a low coherent ratio, we carried out calculations of the static structure factor $S(Q)$ for hydrated pGFP and dGFP ($h = 0.4$), using the 6l26 PDB structure of a mutant enhanced GFP collected at $T = 100$ K by Shibazaki *et al.* [51,52] with neutron diffraction at a space resolution of 1.45 Å and displaying explicit hydrogen nuclei positions, labile protons [49], and hydration water (see Sec. III B 1 of the SM [20]). Hydration water was further generated with SOLVATE software [53], minimizing steric constraints, and compared to crystallographic water (see Fig. S4 of the SM [20,54]). Calculations were extended over all distances considering an isotropic powder sample

$$S(Q) = \frac{1}{N}\sum_{j,k}\Gamma_{jk}\frac{\sin(Qr_{jk})}{Qr_{jk}}, \tag{16}$$

where r_{jk} is the scalar distance between two nuclei, and N the total number of nuclei. We consider that all fast-labile atoms (exchange rate constant $k \approx 10^{-1}$ s^{-1} [55]) and slow-exchanging amide backbone protons ($k \in [10^{-2}, 10^{-9}]$ s^{-1} in lysozyme [56]) have exchanged.

It appears that for hydrated dGFP, sole labile atoms exchange, again, cannot explain the strong discrepancy between the asymptotic and the experimental ratio (see the gray curve

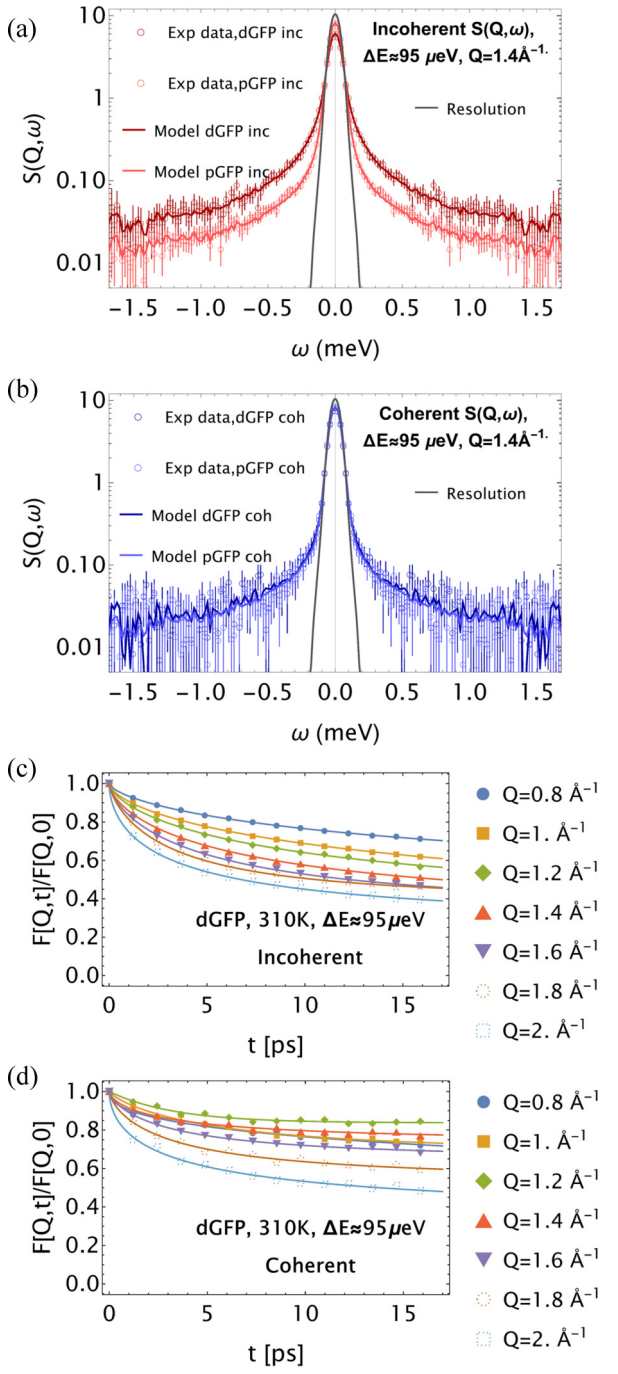

FIG. 3. Scattering functions obtained on LET with polarization analysis, $\Delta E \approx 95$ μeV and $T = 310$ K. [(a) and (b)] Experimental (open dots) and modeled (lines) dynamical structure factors $S(Q, \omega)$ are compared for dGFP and pGFP in the case of incoherent scattering [(a), red] and coherent scattering [(b), blue], for $Q = 1.4$ Å^{-1}. [(c) and (d)] Markers display the experimental intermediate scattering function $F(Q, t)$ obtained for $Q \in [1, 2]$ Å^{-1}, plotted for the dGFP sample only. The fitted model expressed in Eqs. (7) and (11) is shown with solid lines. (c) Incoherent scattering, (d) coherent scattering.

in Fig. 2). An amount of approximately 40% D → H exchange in hydration water is required to match experiments (see the black curve in Fig. 2). Low Q discrepancies arise because calculations are performed on a single protein; hence, the largest interprotein distances equivalent to low Q values are obliterated. This exchange occurs during sample preparation while weighing the sample, before sealing the sample holder (see Sec. I of the SM [20]). It likely points out a consistent subsecond surface hygroscopic $D_2O + H_2O \longleftrightarrow 2$ HDO exchange phenomenon with the atmosphere as already reported in literature to occur at the millisecond scale for a single event in water droplets [57,58]. This is probably enhanced at the protein's interface by surface charges and steric effects. This exchange phenomenon should be considered during sample preparation of hydrated powders.

The use of polarization analysis is key to observing this phenomenon. It might be challenging to trace this effect in standard studies with protonated proteins, due to the negligible impact of increasing water exchange on the coherent to total scattering ratio (see Fig. S5 of the SM [20]). Furthermore, hydration water exchange appears less favorable in the case of pGFP compared to dGFP.

We also compared dGFP and pGFP ω-integrated incoherent intensities (see Fig. S6 of the SM [20]), corroborating the aforementioned results: the same amount of D → H exchanged hydration water is found to explain experimental deviations. It reinforces the insight that the low $S_{coh}(Q)/S_{tot}(Q)$ ratio stems from an increase of incoherent scattering intensity upon D → H exchange. Concomitantly, it rules out another possible explanation, which is that the low intensity of coherent scattering stems from negative, strong cross-correlation terms.

Hence, both the kinetics and the extent of hydration water D → H exchange in protein powders at room temperature and atmospheric pressure are usually underestimated during sample preparation, explaining the low experimental ratio of coherent scattering observed in the deuterated protein.

IV. INCOHERENT QUASIELASTIC SCATTERING OF PROTONATED AND DEUTERATED PROTEIN POWDERS

With this in mind, we investigated the self-dynamics of both pGFP and dGFP with polarized neutrons on LET: it is expected from the previous section that incoherent quasielastic scattering of a deuterated protein is significantly impacted by exchanged water dynamics, due to the large cross section of hydrogen with respect to deuterium ($\sigma_{inc,H} = 80.3$ barns, $\sigma_{inc,D} = 2.05$ barns [2]). However, the impact on the protonated powder should be screened by the amount of slowly relaxing hydrogen atoms in the protein itself $[\sigma_{inc,GFP}/(\sigma_{inc,D_2O+H_2O} + \sigma_{inc,GFP}) = 80\%]$.

For this purpose, $S(Q, \omega)$ experimental data are compared to our fitted model for $Q = 1.4$ Å^{-1} [see Figs. 3(a) and 3(b) for incoherent and coherent scattering, respectively]. The quality of the fit is assessed with $F(Q, t)$ at all Q values for dGFP [see Figs. 3(c) and 3(d)]. Dynamic parameters τ, α, and ESF, fitted with Eq. (7), are displayed in Figs. 4(a) and 4(b). Contributions on Fig. 4 are either separated (incoherent scattering represented with blue dots and coherent scattering with orange dots) or merged (inc + coh, gray lines joining data points). First and foremost, a consequence of D → H exchanges are non-negligible signatures of water self-dynamics in the deuterated protein sample, probed by incoherent scattering with a dynamic timescale $\tau_{inc,dGFP}$ decreasing with Q from

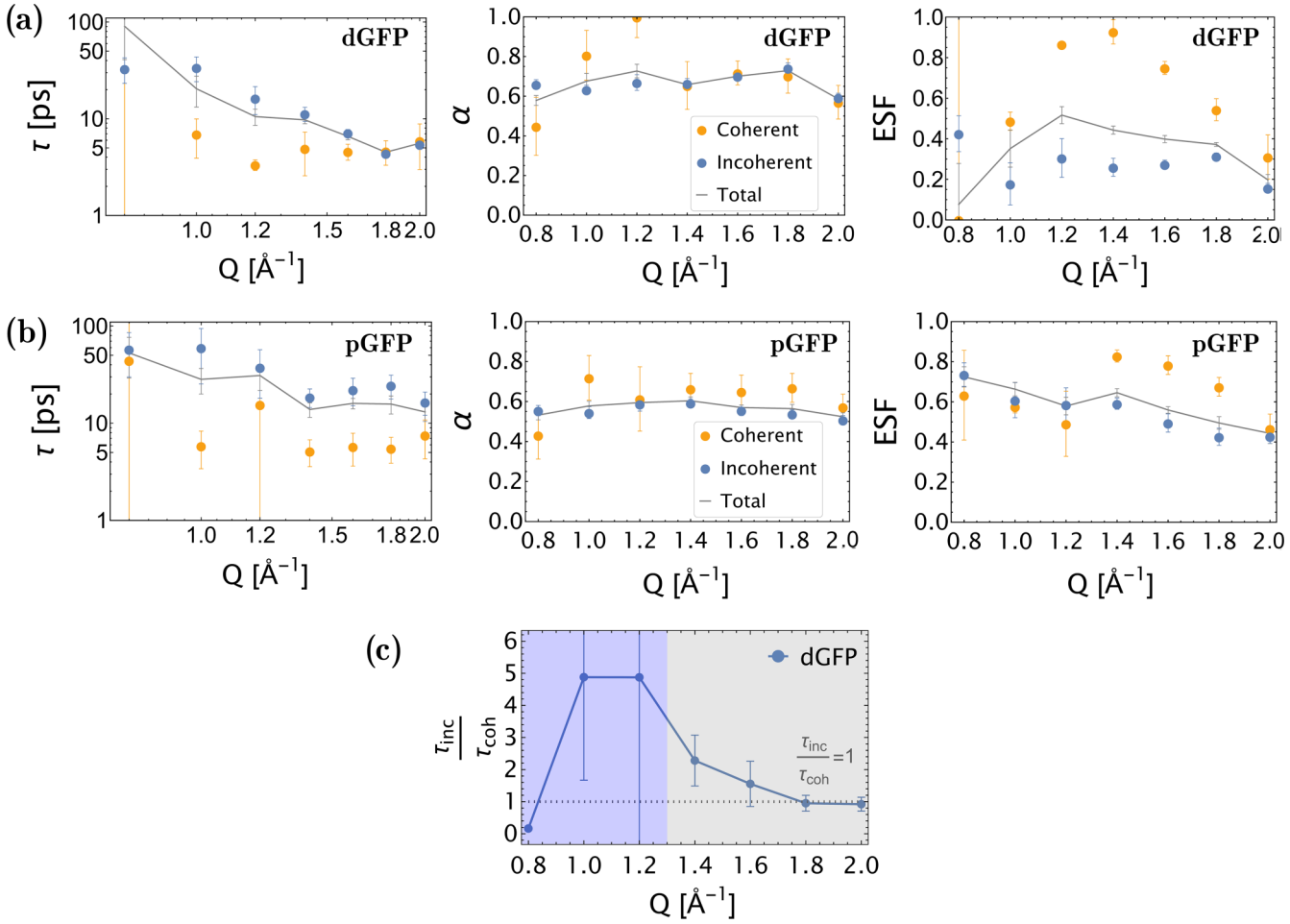

FIG. 4. τ, α, and ESF parameters are displayed for incoherent (blue dots), coherent (orange dots), and merged incoherent + coherent (gray lines) contributions on LET with polarization analysis at $T = 310$ K. [(a) and (b)] Parameters obtained for dGFP and pGFP, respectively. (c) The ratio of incoherent over coherent dynamic timescales, $\tau_{inc}(Q)/\tau_{coh}(Q)$, is plotted for dGFP. The gray dotted line corresponds to $\tau_{inc}(Q)/\tau_{coh}(Q) = 1$, indicating the merge of timescales. The gray area indicates the region where both timescales merge, in contrast to the blue area where they diverge.

about 30 ps ($Q = 1$ Å^{-1}) to about 5 ps ($Q = 2$ Å^{-1}). Indeed, self-diffusion in dGFP H_2O hydration water is reported to occur at the picosecond timescale with a similar Q-dependent relaxation time [19] (the lifetime of a H bond in hydration water is about 2 ps [59]). In the hydration shell, individual relaxation times are distributed according to a power law [39]: this heterogeneity is captured here from the factor $\alpha_{inc,dGFP} \approx 0.66$. In comparison, α is reported to decrease from 1 at large Q values down to 0.9 at $Q = 1$ Å^{-1} for bulk H_2O [34].

The signature of water in dGFP is all the more obvious from the slower relaxation timescale $\tau_{inc,pGFP} > 15$ ps in pGFP, corresponding to the protein itself due to its large proportion of H nuclei. The clear Q dependence of dGFP also denotes a diffusive process, in comparison to pGFP. Hence, pGFP dynamics arises from highly local motions of hydrogen nuclei in the residues, as noticed earlier in powder-state GFP [60] due to the rigidity of this β barrel protein [61]. Moreover, density fluctuations in the pGFP sample diffuse in an energy landscape displaying a rugged surface compared to the dGFP sample (see Sec. II D of the SM [20]), with $\alpha_{inc,dGFP} \approx \alpha_{inc,pGFP} + 0.12$. This is because hydration water dynamics is softer than GFP dynamics, which is reported with similar stretching exponents by Nickels *et al.* [19,60].

The slow and heterogeneous dynamics in pGFP compared to dGFP cannot be attributed to an "isotope effect" taking place in the protein's internal dynamics. Currently, although studies report a clear solvent isotope effect in D_2O compared to H_2O that stiffens the protein [62–64], the effect of the protein's perdeuteration on its dynamics is still unclear and is reported to depend on proteins or regions inside the proteins [65], as well as timescales under study [66,67]. Indeed, even in a light system such as water, isotopic exchange induces only a $D_{D_2O}/D_{H_2O} \approx 1.2$ ratio for the translational diffusion coefficient D at 310 K [68–70], and remains below 1.15 in many liquids for both rotational and translational diffusion [71], while we get $\tau_{inc,pGFP}/\tau_{inc,dGFP} \approx 3$.

It is thus reasonable to admit that dGFP incoherent scattering is strongly overtaken by the H-bond network dynamics of exchanged water. Hence, it is paramount to any neutron experimenter to keep in mind that even low exchange ratios in the hydration layer of a perdeuterated powder compound lead to a dominance of hydration dynamics on the picosecond scale

for incoherent scattering, which prevents any isotope effect studies.

V. COHERENT DYNAMICS IN PROTEINS AT THE PICOSECOND TIMESCALE ARE OVERTAKEN BY HYDRATION WATER DYNAMICS

While incoherent scattering favors the visibility of hydrogen and to a lower extent deuterium atoms, all nuclei are weighted similarly in coherent scattering [2]. Therefore, reasoning from a "static" point of view, a large contribution from the protein itself is expected in the coherent channel (see Fig. S2 of the SM [20]), of 69% for pGFP and 74% for dGFP, respectively. It implies a significant role of all nuclei types in the protein, which is barely affected by D → H exchange in hydration water. Hence, it implies that collective dynamics of the protein should dominate.

However, experiments suggest that collective motions mostly arise from deuterium and oxygen nuclei motions in the hydration layer in both protein samples. Indeed, the τ_{coh} parameter unravels faster dynamics compared to incoherent scattering [see Figs. 4(a) and 4(b)]. Parameters are almost identical within error bars for pGFP and dGFP with $\tau_{\mathrm{coh}} \approx 5$ ps and $\alpha_{\mathrm{coh}} \approx 0.65$ (see Fig. S8(b) of the SM [20]). This is in agreement with the timescale $\tau_{\mathrm{collective}} \approx 4$ ps of the local collective relaxation of the first hydration layer of apomyoglobin obtained with femtosecond fluorescence Stokes shift spectroscopy [72–74], and much faster than the timescales expected for backbone and full side-chain dynamics in the protein [75]. Hence, internal protein motions arising from heavy atoms are negligible in the coherent signal, and dynamics stems from structural relaxation in hydration water.

Let us now mention a striking feature which is the almost Q-independent timescale τ_{coh} of structural relaxation. It has been observed by Arbe and collaborators with polarized experiments and simulations of coherent neutron scattering in bulk D_2O [14,76] and van der Waals liquids [16]. It has been assigned to a local mode that they identify with H-bond forming and breaking leading to the relaxation of the H-bond network in D_2O [14]. In Refs. [15,76], Alvarez *et al.* used molecular dynamics simulations to rationalize the absence of diffusive behavior in the low-Q range: the diffusive component contained in both self- and distinct partial dynamical structure factors bears opposite signs until $Q < 1.5$ Å^{-1} where a strong correlation peak emerges. Hence, diffusion cancels and only the local process remains. Yet, we do not observe opposite trends for self- and distinct coherent scattering in our calculated partial static structure factors for hydration water (see Fig. S4 of the SM [20]) to put forward a similar explanation. Still, strong discrepancies between incoherent and coherent scattering of dGFP are observed for low Q values, implying that if water is indeed the main contribution in both channels, then distinct (purely collective) scattering is clearly non-negligible. Furthermore, we notice that this scale-independent τ_{coh} is associated to an almost Q-independent coherent relaxation function $\phi_{\mathrm{coh}}(Q,t)$, as has been observed with experiments and simulations for transient polymer networks or supercooled water at mesoscopic Q values [14,77,78] (see Fig. S9 of the SM [20]). Therefore, the characteristics of coherent scattering in hydration water are reminiscent of collective dynamics in other complex systems: it appears that a local process prevails, rather than diffusive dynamics.

In that sense, we do not observe any scaling of τ_{coh} with $S(Q)$ that could be assigned to a de Gennes narrowing [79]. This principle based on sum rules formulates that the coherent relaxation timescale increases due to space correlations around the main diffraction peak. It has been observed for complex systems with heterogeneous dynamics (glassy liquids [16,80,81] or multidomain proteins [82]). However, it was not observed in D_2O [14]. Nevertheless, the heterogeneity parameter α_{coh} and more convincingly the elastic coherent structure factor (ECSF) follow the trend of $S(Q)$ where structural correlations are maximal around $Q = 1.4$ Å^{-1}, indicating that coherent parameters share similar behaviors with glass-forming liquids [81]. This is a direct expression of the impact of structure in collective processes. We also notice that the ECSF is much larger and closer to 1 compared to the EISF, due to the large amount (1/3 of all nuclei) of heavy atoms which are invisible to incoherent scattering but enter the signal for coherent scattering and appear immobile at our energy resolution.

It is further corroborated that incoherent and coherent scattering in dGFP both correspond to hydration water: just as Arbe *et al.* observe for D_2O, there is a merge of incoherent and coherent timescales of motions in dGFP [14] [Fig. 4(c)] at short distances in the range of noncovalent bonds when $Q \geqslant 1.4$ Å^{-1}.

In order to characterize the confinement effect of hydration water with respect to bulk water, we calculate a collective retardation factor for D_2O:

$$\xi_{\mathrm{D_2O,\,coh}} = \frac{\tau_{\mathrm{D_2O,hydr,coh}}}{\tau_{\mathrm{D_2O,bulk,coh}}} \approx 2.5 \tag{17}$$

is scale-free, contrary to the Q-dependent incoherent retardation factor obtained for H_2O hydration water in GFP by Perticaroli *et al.* [19], which increases strongly when Q decreases. $\tau_{\mathrm{D_2O,bulk,coh}}$ is extracted from Ref. [14] while $\tau_{\mathrm{D_2O,hydr,coh}}$ corresponds to either the pGFP or dGFP τ_{coh} parameter. This is supported by the fact that the same magnitudes for self- [19] and collective retardation factors are recovered for $Q \approx 2$ Å^{-1}. However, this comparison is model limited: our model corresponds to a widespread distribution of exponential relaxations (see Sec. II D and Fig. S1 of the SM [20]), while Arbe *et al.* propose a biexponential relaxation. In conclusion, coherent scattering of a protein powder at the picosecond timescale is strongly overtaken by confined heavy-water fast collective dynamics, which display a Q-independent relaxation time as observed in bulk D_2O with polarized neutron scattering. It corresponds to a local H-bond breaking and forming process. In hydration water, this dynamics is slowed down with respect to bulk D_2O.

VI. IMPACT OF WATER COLLECTIVE MOTIONS ON DYNAMIC PARAMETERS

Figures 5(a) and 5(b) express the errors made if the experimenter uses a nonpolarized beam when assessing self-diffusion:

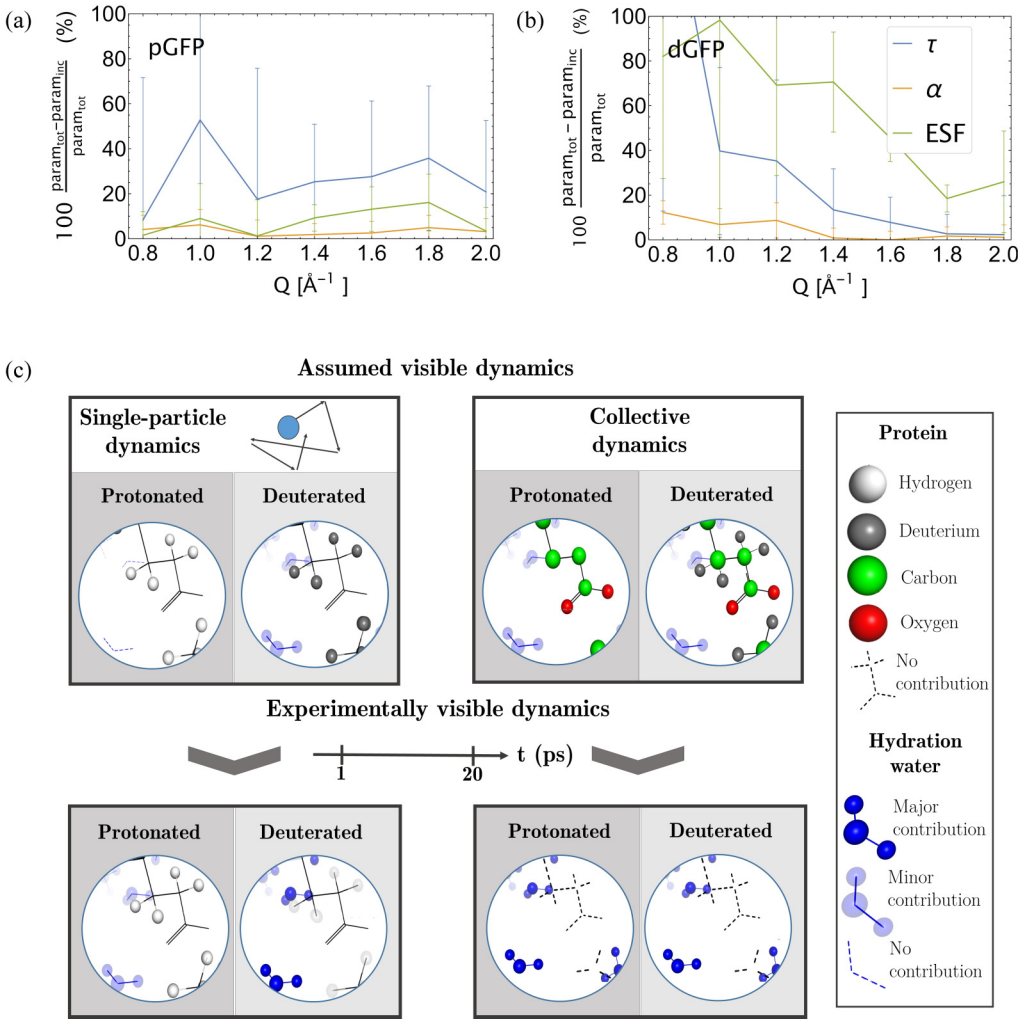

FIG. 5. Relative gaps for dynamic parameters τ (blue), α (orange line), and ESF (green line) as a function of Q, corresponding to the error made using a nonpolarized beam (inc + coh) compared to polarized incoherent scattering, for (a) pGFP and (b) dGFP. (c) Dynamics expected to prevail in the sample using usual self-cross-section arguments (15) are displayed in the upper panel and divided into incoherent (self-) dynamics and coherent (collective) dynamics. Opacity identifies which species or atoms provide major contributions, while transparency and dashes express minor and nonexistent contributions, respectively; see the chart on the right. Colors designate different atomic types. The lower panel maps the effective dynamics that prevail in the sample, as analyzed from polarized neutron scattering for $t \in [1, 16]$ ps and $Q \geqslant 1$ Å^{-1}. The figure is produced with PYMOL software [83] with a 4-Å-diam focus on GLU34.

(i) The impact of coherent scattering on the protonated protein is due to the fast picosecond fluctuations of the collective motions of the hydrogen-bond network of water. It artificially decreases the relaxation timescale of the slow and heterogeneous self-dynamics of proteins. It therefore mainly impacts τ (in blue) by about 30%, but it leaves α (in orange) and the ESF (in green) almost identical ($\leqslant$5% and $\leqslant$10%) [Fig. 5(a)].

(ii) The impact of collective dynamics on total scattering is more important for the deuterated protein. The ESF is poorly estimated on the whole Q range, whereas τ is almost retrieved at higher Q. α is subject to an error below 10%. The question still remains for the error made on a deuterated protein in D_2O if no D $\rightarrow$ H exchange occurs [Fig. 5(b)].

Therefore, for both samples it implies a systematic underestimation of the timescale of motions and an underestimation of the heterogeneity in the sample, while the impact on the asymptotic regime is less measurable. For pGFP, the error performed on the ESF is close to 10% as already observed in protonated or partially deuterated polymers [84,85], while it is the least-correctly estimated parameter for dGFP due to the presence of heavy scatterers in coherent scattering. At $Q = 0.8$ Å^{-1} the trend seems to exchange suddenly in both samples, with a strong increase of coherent timescales and decrease of heterogeneity. However, statistics are not good enough to infer if it is due to the entrance of backbone and side-chain motions at larger scales.

Molecular dynamics simulations performed on D_2O hydrated lysozyme for $t < 50$ ps by Matsuo [86] suggest less than 6% of discrepancy between incoherent and total dynamic parameters (jump diffusion model) for the protein only. Therefore, it seems that hydration water dynamics play a strong role in widening the gap between incoherent and total dynamic parameters in experiments.

A schematic in Fig. 5(c) sums up the interpretations provided in Secs. IV and V. Except for incoherent scattering of a protonated protein, which is the usual configuration studied by neutron scattering experimenters, incoherent scattering of a perdeuterated protein and coherent scattering of both a protonated and a perdeuterated protein all present a strong mismatch between assumed dynamics and experimentally probed dynamics on the picosecond range. It proves that perdeuteration of a protein sample at this resolution, even with clear separation of the coherent contribution, is a disputable probe of the collective motions of the protein itself.

VII. CONCLUSION

We applied a minimalist model accounting for non-Markovian dynamics to capture the highly heterogeneous dynamics of both a protein and its hydration water probed with polarized QENS.

We demonstrated that dynamics in a hydrated protein powder probed at the picosecond timescale is highly contaminated by the fast collective motions of the heavy-water D-bond network, although deuteration of the hydration layer is used in principle for the purpose of enhancing the protein's dynamics against its solvent. This holds for both a protonated and a perdeuterated protein in D_2O. Although the intensity of coherent scattering is low compared to incoherent scattering, there is a strong mismatch when the beam is unpolarized due to the difference in timescales of water and protein dynamics.

It puts into perspective the relevance of deuteration as a contrast tool for neutron scattering, depending on the momentum and energy transfer scales studied. It also questions using solely the ratios of coherent and incoherent atomic bound cross sections, which hold for "static" studies such as diffraction, to deduce which parts of the sample will be highlighted in the case of energy-dependent neutron spectroscopy experiments.

Furthermore, the deuteration process of a protein hydration layer is questioned from polarized neutron diffraction, pointing out very fast (less than a second) D/H exchange upon exposure to the atmosphere. We reckon that D_2O adsorption should be performed systematically under controlled hydrogen-free atmosphere to avoid contamination from hydrogen nuclei in the hydration layer of the powder-state protein (this issue might not arise in solutions due to the slow exchange time of deuterated bulk water [87] compared to interface water).

Our insights might be extended to the impact of collective water dynamics in a protein solution as well, for which the Q-dependent retarded first hydration layer cannot be subtracted from a bulk-water spectrum. Moreover, the impact of coherent scattering on the total signal increases at lower Q scales where the coherent fraction of scattering can be preponderant due to water-protein and protein-protein correlations [13], raising the question of the choice of the Q range to avoid prominent contamination from coherent scattering. Identically, the study of slower relaxation times using higher energy resolutions should modify the relative impact of the solvent on the dynamics of the protein sample.

We want to point out that our results may vary with secondary structure, since GFP is known as a particularly stiff protein due to its β barrel structure [61].

Data is accessible from Ref. [88–90].

ACKNOWLEDGMENTS

We have benefited from the strong support of Elisabetta Boeri, who ran mass spectrometry measurements on the IBS mass spectrometry platform, IBS, Instruct-ERIC center (ISBG; UAR 3518 CNRS-CEA-UGA-EMBL) within the Grenoble Partnership for Structural Biology (PSB), supported by FRISBI (Grant No. ANR-10-INBS-0005-02) and GRAL, financed within the University Grenoble Alpes graduate school (Ecoles Universitaires de Recherche) CBH-EUR-GS (Grant No. ANR-17-EURE-0003). We also thank Tatsuhito Matsuo for discussions and support. We thank Institut Laue-Langevin, Grenoble, France, for beam-time allowance on D7 and IN12 instruments, as well as the ISIS neutron facility for beam-time allowance on LET. We gratefully acknowledge financial support from Mission pour les Initiatives Transverses et Interdisciplinaires du CNRS, BioQuant, attributed to J.P. We acknowledge as well the Ph.D. grant attributed to A.N., delivered by Ministère de l'Éducation nationale, de l'Enseignement supérieur et de la Recherche (MENESR-ED).

[1] M. Bee, *Quasielastic Neutron Scattering, Principles and Applications in Solid State Chemistry, Biology and Materials Science* (CRC Press, London, 1988).

[2] V. F. Sears, Neutron scattering lengths and cross sections, Neutron News **3**, 26 (1992).

[3] M. Haertlein, M. Moulin, J. M. Devos, V. Laux, O. Dunne, and V. T. Forsyth, Biomolecular deuteration for neutron structural biology and dynamics, in *Methods in Enzymology* (Elsevier, Amsterdam, 2016), Vol. 566, pp. 113–157.

[4] K. Wood, A. Frölich, A. Paciaroni, M. Moulin, M. Härtlein, G. Zaccai, D. J. Tobias, and M. Weik, Coincidence of dynamical transitions in a soluble protein and its hydration water: Direct measurements by neutron scattering and MD simulations, J. Am. Chem. Soc. **130**, 4586 (2008).

[5] M.-C. Bellissent-Funel, J. Teixeira, K. F. Bradley, and S. H. Chen, Dynamics of hydration water in protein, J. Phys. I **2**, 995 (1992).

[6] J. D. Nickels, H. O'Neill, L. Hong, M. Tyagi, G. Ehlers, K. L. Weiss, Q. Zhang, Z. Yi, E. Mamontov, J. C. Smith *et al.*, Dynamics of protein and its hydration water: Neutron scattering studies on fully deuterated GFP, Biophys. J. **103**, 1566 (2012).

[7] L. Hong, N. Jain, X. Cheng, A. Bernal, M. Tyagi, and J. C. Smith, Determination of functional collective motions in a protein at atomic resolution using coherent neutron scattering, Sci. Adv. **2**, e1600886 (2016).

[8] J. D. Nickels, S. Perticaroli, H. O'Neill, Q. Zhang, G. Ehlers, and A. P. Sokolov, Coherent neutron scattering and collective dynamics in the protein, GFP, Biophys. J. **105**, 2182 (2013).

[9] M. Bellissent-Funel, A. Filabozzi, and S. Chen, Measurement of coherent Debye-Waller factor in in vivo deuterated C-phycocyanin by inelastic neutron scattering, Biophys. J. **72**, 1792 (1997).

[10] G. Nilsen, J. Kosata, M. Devonport, P. Galsworthy, R. Bewley, D. Voneshen, R. Dalgliesh, and J. Stewart, Polarisation analysis on the LET time-of-flight spectrometer, J. Phys.: Conf. Ser. **862**, 012019 (2017).

[11] B. J. Gabrys, Applications of polarized neutrons to non-magnetic materials, Phys. B: Condens. Matter **267–268**, 122 (1999).

[12] J. R. Stewart, P. P. Deen, K. H. Andersen, H. Schober, J.-F. Barthélémy, J. M. Hillier, A. P. Murani, T. Hayes, and B. Lindenau, Disordered materials studied using neutron polarization analysis on the multi-detector spectrometer, D7, J. Appl. Crystallogr. **42**, 69 (2009).

[13] A. M. Gaspar, S. Busch, M.-S. Appavou, W. Haeussler, R. Georgii, Y. Su, and W. Doster, Using polarization analysis to separate the coherent and incoherent scattering from protein samples, Biochim. Biophys. Acta: Proteins Proteomics **1804**, 76 (2010).

[14] A. Arbe, G. J. Nilsen, J. R. Stewart, F. Alvarez, V. G. Sakai, and J. Colmenero, Coherent structural relaxation of water from meso- to intermolecular scales measured using neutron spectroscopy with polarization analysis, Phys. Rev. Res. **2**, 022015(R) (2020).

[15] F. Alvarez, A. Arbe, and J. Colmenero, Unraveling the coherent dynamic structure factor of liquid water at the mesoscale by molecular dynamics simulations, J. Chem. Phys. **155**, 244509 (2021).

[16] A. Arbe, G. J. Nilsen, M. Devonport, B. Farago, F. Alvarez, J. A. Martínez González, and J. Colmenero, Collective dynamics and self-motions in the van der Waals liquid tetrahydrofuran from meso- to inter-molecular scales disentangled by neutron spectroscopy with polarization analysis, J. Chem. Phys. **158**, 184502 (2023).

[17] T. Burankova, J. F. M. Cardozo, D. Rauber, A. Wildes, and J. P. Embs, Linking structure to dynamics in protic ionic liquids: A neutron scattering study of correlated and single-particle motions, Sci. Rep. **8**, 16400 (2018).

[18] T. Burankova, R. Hempelmann, A. Wildes, and J. P. Embs, Collective ion diffusion and localized single particle dynamics in pyridinium-based ionic liquids, J. Phys. Chem. B **118**, 14452 (2014).

[19] S. Perticaroli, G. Ehlers, C. B. Stanley, E. Mamontov, H. O'Neill, Q. Zhang, X. Cheng, D. A. A. Myles, J. Katsaras, and J. D. Nickels, Description of hydration water in protein (green fluorescent protein) solution, J. Am. Chem. Soc. **139**, 1098 (2017).

[20] See Supplemental Material at http://link.aps.org/supplemental/10.1103/PRXLife.2.013005 for Section I describes sample preparation, which includes Refs. [3,19,21,22,49]. Section II includes details on neutron scattering experiments, instruments' characteristics, and data reduction and analysis, which includes Refs. [8,10,12–14,23–32,47,48,91,92] and Fig. S1. Section. III provides more information on the calculations performed to obtain $S(Q)$, the treatment of the hydration layer, and further evidence towards strong H/D exchange in the hydration layer, which includes Refs. [7,51–54,64,93] and Figs. S2–S7. Section IV is used to provide comparison of incoherent and coherent scattering parameters, which includes Fig. S8. It also features the Q dependence of fitted relaxation functions, Fig. S9.

[21] F. Bernaudat and L. Bülow, Combined hydrophobic-metal binding fusion tags for applications in aqueous two-phase partitioning, Protein Expression Purif. **46**, 438 (2006).

[22] R. Zorn, Multiple scattering correction of polarized neutron diffraction data, Nucl. Instrum. Methods Phys. Res. Sect. A **479**, 568 (2002).

[23] K. Schmalzl, W. Schmidt, S. Raymond, H. Feilbach, C. Mounier, B. Vettard, and T. Brueckel, The upgrade of the cold neutron three-axis spectrometer IN12 at the ILL, Nucl. Instrum. Methods Phys. Res. Sect. A **819**, 89 (2016).

[24] R. Bewley, J. Taylor, and S. Bennington., LET, a cold neutron multi-disk chopper spectrometer at ISIS, Nucl. Instrum. Methods Phys. Res. Sect. A **637**, 128 (2011).

[25] J. Košata, G. Nilsen, M. Devonport, R. Bewley, D. Voneshen, P. Galsworthy, D. Raspino, and J. Stewart, Polarized primary spectrometer on the LET instrument at ISIS, Phys. B: Condens. Matter **551**, 476 (2018).

[26] D. Richard, M. Ferrand, and G. Kearley, Analysis and visualisation of neutron-scattering data, J. Neutron Res. **4**, 33 (1996).

[27] O. Arnold, J. Bilheux, J. Borreguero, A. Buts, S. Campbell, L. Chapon, M. Doucet, N. Draper, R. F. Leal, M. Gigg, V. Lynch, A. Markvardsen, D. Mikkelson, R. Mikkelson, R. Miller, K. Palmen, P. Parker, G. Passos, T. Perring, P. Peterson *et al.*, Mantid–Data analysis and visualization package for neutron scattering and μSR experiments, Nucl. Instrum. Methods Phys. Res. Sect. A **764**, 156 (2014).

[28] Wolfram Inc., *Mathematica*, Version 13.2, Champaign, IL, 2022.

[29] R. Zorn, Sample shape contribution to the resolution function of time-of-flight neutron scattering spectrometers, Nucl. Instrum. Methods Phys. Res. Sect. A **674**, 85 (2012).

[30] M. Saouessi, J. Peters, and G. R. Kneller, Asymptotic analysis of quasielastic neutron scattering data from human acetylcholinesterase reveals subtle dynamical changes upon ligand binding, J. Chem. Phys. **150**, 161104 (2019).

[31] A. N. Hassani, L. Haris, M. Appel, T. Seydel, A. M. Stadler, and G. R. Kneller, Multiscale relaxation dynamics and diffusion of myelin basic protein in solution studied by quasielastic neutron scattering, J. Chem. Phys. **156**, 025102 (2022).

[32] A. N. Hassani, A. M. Stadler, and G. R. Kneller, Quasi-analytical resolution-correction of elastic neutron scattering from proteins, J. Chem. Phys. **157**, 134103 (2022).

[33] P. Schofield, Space-time correlation function formalism for slow neutron scattering, Phys. Rev. Lett. **4**, 239 (1960).

[34] M. H. Petersen, M. T. Telling, G. Kneller, and H. N. Bordallo, Revisiting the modeling of quasielastic neutron scattering from bulk water, EPJ Web Conf. **272**, 01012 (2022).

[35] G. R. Kneller, Franck-Condon picture of incoherent neutron scattering, Proc. Natl. Acad. Sci. USA **115**, 9450 (2018).

[36] W. Min, G. Luo, B. J. Cherayil, S. C. Kou, and X. S. Xie, Observation of a power-law memory kernel for fluctuations within a single protein molecule, Phys. Rev. Lett. **94**, 198302 (2005).

[37] J. Schlichter, J. Friedrich, L. Herenyi, and J. Fidy, Protein dynamics at low temperatures, J. Chem. Phys. **112**, 3045 (2000).

[38] K. Kämpf, F. Klameth, and M. Vogel, Power-law and logarithmic relaxations of hydrated proteins: A molecular dynamics simulations study, J. Chem. Phys. **137**, 205105 (2012).

[39] A. C. Fogarty and D. Laage, Water dynamics in protein hydration shells: The molecular origins of the dynamical perturbation, J. Phys. Chem. B **118**, 7715 (2014).

[40] I. E. T. Iben, D. Braunstein, W. Doster, H. Frauenfelder, M. K. Hong, J. B. Johnson, S. Luck, P. Ormos, A. Schulte, P. J. Steinbach, A. H. Xie, and R. D. Young, Glassy behavior of a protein, Phys. Rev. Lett. **62**, 1916 (1989).

[41] H. Frauenfelder, S. G. Sligar, and P. G. Wolynes, The energy landscapes and motions of proteins, Science **254**, 1598 (1991).

[42] W. G. Glöckle and T. F. Nonnenmacher, A fractional calculus approach to self-similar protein dynamics, Biophys. J. **68**, 46 (1995).

[43] R. Zwanzig, *Lectures in Theoretical Physics* (Wiley, New York, 1961), pp. 139–172.

[44] R. Zwanzig, *Nonequilibrium Statistical Mechanics* (Oxford University Press, Oxford, UK, 2001).

[45] *Mittag-Leffler Functions, Related Topics and Applications*, edited by R. Gorenflo, A. A. Kilbas, F. Mainardi, and S. V. Rogosin, Springer Monographs in Mathematics (Springer, Heidelberg, 2014).

[46] F. Mainardi, Why the Mittag-Leffler function can be considered the queen function of the fractional calculus? Entropy **22**, 1359 (2020).

[47] W. Zajac, Structure of poly(ethylene oxide) (PEO and PEO · $LiSO_3CF_3$) studied with spin polarised neutrons, Solid State Ionics **147**, 213 (2002).

[48] B. Gabryś and O. Schärpf, Scattering from polymers using polarised neutrons: A new development, Phys. B: Condens. Matter **180-181**, 495 (1992).

[49] Y. Efimova, A. van Well, U. Hanefeld, B. Wierczinski, and W. Bouwman, On the neutron scattering length density of proteins in H_2O/D_2O, Phys. B: Condens. Matter **350**, E877 (2004).

[50] M.-C. Bellissent-Funel, J. Lal, K. Bradley, and S. Chen, Neutron structure factors of in-vivo deuterated amorphous protein C-phycocyanin, Biophys. J. **64**, 1542 (1993).

[51] C. Shibazaki, R. Shimizu, Y. Kagotani, A. Ostermann, T. E. Schrader, and M. Adachi, Direct observation of the protonation states in the mutant green fluorescent protein, J. Phys. Chem. Lett. **11**, 492 (2020).

[52] M. Adachi, R. Shimizu, C. Shibazaki, Y. Kagotani, A. Ostermann, and T. Schrader, Neutron crystal structure of the mutant green fluorescent protein (EGFP) (2020), https://doi.org/10.2210/pdb6l26/pdb.

[53] H. Grubmüller, SOLVATE, Theoretical Biophysics Group, Institut für Medizinische Optik, Ludwig-Maximilians-Universität München, München, Germany, https://www.mpinat.mpg.de/628104/07-License.

[54] M. Bin, R. Yousif, S. Berkowicz, S. Das, D. Schlesinger, and F. Perakis, Wide-angle x-ray scattering and molecular dynamics simulations of supercooled protein hydration water, Phys. Chem. Chem. Phys. **23**, 18308 (2021).

[55] J. A. Brockerman, Characterizing labile protons by NMR spectroscopy, Ph.D. thesis, University of British Columbia (2019).

[56] S. E. Radford, M. Buck, K. D. Topping, C. M. Dobson, and P. A. Evans, Hydrogen exchange in native and denatured states of hen egg-white lysozyme, Proteins: Struct. Funct. Genet. **14**, 237 (1992).

[57] S. Maithani, A. Maity, and M. Pradhan, Probing the H to D isotopic exchange reaction in a liquid droplet via surface plasmon resonance, J. Anal. At. Spectrom. **37**, 544 (2022).

[58] T.-S. Kim, H. Park, K. Ko, G. Lim, Y.-H. Cha, J. Han, and D.-Y. Jeong, Laser-based sensor for a coolant leak detection in a nuclear reactor, Appl. Phys. B **100**, 437 (2010).

[59] M. Maurer and C. Oostenbrink, Water in protein hydration and ligand recognition, J. Mol. Recognit. **32**, e2810 (2019).

[60] J. D. Nickels, V. García Sakai, and A. P. Sokolov, Dynamics in protein powders on the nanosecond-picosecond time scale are dominated by localized motions, J. Phys. Chem. B **117**, 11548 (2013).

[61] S. Perticaroli, J. D. Nickels, G. Ehlers, H. O'Neill, Q. Zhang, and A. P. Sokolov, Secondary structure and rigidity in model proteins, Soft Matter **9**, 9548 (2013).

[62] S.-Y. Sheu, E. W. Schlag, H. L. Selzle, and D.-Y. Yang, Molecular dynamics of hydrogen bonds in protein-D_2O: The solvent isotope effect, J. Phys. Chem. A **112**, 797 (2008).

[63] M. Jasnin, M. Tehei, M. Moulin, M. Haertlein, and G. Zaccai, Solvent isotope effect on macromolecular dynamics in *E. coli*, Eur. Biophys. J. **37**, 613 (2008).

[64] Y. M. Efimova, S. Haemers, B. Wierczinski, W. Norde, and A. A. van Well, Stability of globular proteins in H_2O and D_2O, Biopolymers **85**, 264 (2007).

[65] P. J. Nichols, I. Falconer, A. Griffin, C. Mant, R. Hodges, C. J. McKnight, B. Vögeli, and L. Vugmeyster, Deuteration of nonexchangeable protons on proteins affects their thermal stability, side-chain dynamics, and hydrophobicity, Protein Sci. **29**, 1641 (2020).

[66] J. Ramos, V. Laux, M. Haertlein, E. B. Erba, K. E. McAuley, V. T. Forsyth, E. Mossou, S. Larsen, and A. E. Langkilde, Structural insights into protein folding, stability and activity using in vivo perdeuteration of hen egg-white lysozyme, IUCrJ **8**, 372 (2021).

[67] L. Vugmeyster, A. Griffin, D. Ostrovsky, S. Bhattacharya, P. J. Nichols, C. J. McKnight, and B. Vögeli, Correlated motions of C'-N and C_α-C_β pairs in protonated and per-deuterated GB3, J. Biomol. NMR **72**, 39 (2018).

[68] A. Stefaniuk, S. Gawinkowski, B. Golec, A. Gorski, K. Szutkowski, J. Waluk, and J. Poznański, Isotope effects observed in diluted D_2O/H_2O mixtures identify HOD-induced low-density structures in D_2O but not H_2O, Sci. Rep. **12**, 18732 (2022).

[69] F. Prielmeier, E. Lang, R. Speedy, and H.-D. Lüdemann, The pressure dependence of self diffusion in supercooled light and heavy water, Ber. Bunsenges Phys. Chem. **92**, 1111 (1988).

[70] R. Mills, Self-diffusion in normal and heavy water in the range 1-45.deg, J. Phys. Chem. **77**, 685 (1973).

[71] M. Holz, X. Mao, D. Seiferling, and A. Sacco, Experimental study of dynamic isotope effects in molecular liquids: Detection of translation-rotation coupling, J. Chem. Phys. **104**, 669 (1996).

[72] T. Li, A. A. Hassanali, Y.-T. Kao, D. Zhong, and S. J. Singer, Hydration dynamics and time scales of coupled water-protein fluctuations, J. Am. Chem. Soc. **129**, 3376 (2007).

[73] L. Zhang, Y. Yang, Y.-T. Kao, L. Wang, and D. Zhong, Protein hydration dynamics and molecular mechanism of coupled water-protein fluctuations, J. Am. Chem. Soc. **131**, 10677 (2009).

[74] Y. Qin, L. Wang, and D. Zhong, Dynamics and mechanism of ultrafast water-protein interactions, Proc. Natl. Acad. Sci. USA **113**, 8424 (2016).

[75] M. Grimaldo, F. Roosen-Runge, F. Zhang, F. Schreiber, and T. Seydel, Dynamics of proteins in solution, Q. Rev. Biophys. **52**, e7 (2019).

[76] F. Alvarez, A. Arbe, and J. Colmenero, Understanding the coherent dynamic structure factor of liquid water measured by neutron spectroscopy with polarization analysis: A molecular dynamics simulations study, EPJ Web Conf. **272**, 01011 (2022).

[77] P. H. Handle, L. Rovigatti, and F. Sciortino, Independent slow dynamics in atomic and molecular systems, Phys. Rev. Lett. **122**, 175501 (2019).

[78] G. Nava, M. Rossi, S. Biffi, F. Sciortino, and T. Bellini, Fluctuating elasticity mode in transient molecular networks, Phys. Rev. Lett. **119**, 078002 (2017).

[79] P. D. Gennes, Liquid dynamics and inelastic scattering of neutrons, Physica **25**, 825 (1959).

[80] C. Alba-Simionesco, A. Toelle, D. Morineau, B. Farago, and G. Coddens, "de Gennes" narrowing in supercooled molecular liquids: Evidence for center-of-mass dominated slow dynamics, arXiv:cond-mat/0103599.

[81] P. Luo, Y. Zhai, P. Falus, V. G. Sakai, M. Hartl, M. Kofu, K. Nakajima, A. Faraone, and Y. Z, Q-dependent collective relaxation dynamics of glass-forming liquid $Ca_{0.4}K_{0.6}(NO_3)_{1.4}$ investigated by wide-angle neutron spin-echo, Nat. Commun. **13**, 2092 (2022).

[82] L. Hong, N. Smolin, and J. C. Smith, de Gennes narrowing describes the relative motion of protein domains, Phys. Rev. Lett. **112**, 158102 (2014).

[83] L. L. L. Schrödinger, The PyMOL Molecular Graphics System, Version 1.8, New York, NY, USA (2015).

[84] B. Gabrys, J. S. Higgins, and O. Schärpf, Contamination by coherent scattering of the elastic incoherent structure factor observed in neutron scattering experiments, J. Chem. Soc., Faraday Trans. 1 **82**, 1923 (1986).

[85] B. J. Gabrys, W. Zajac, and O. Schärpf, QENS from soft systems: Why use polarised neutrons? Phys. B: Condens. Matter **301**, 69 (2001).

[86] T. Matsuo, Changes in protein dynamical parameters derived from quasi-elastic neutron scattering spectra induced by coherent scattering: A molecular dynamics simulation study, bioRxiv 2022.10.27.514007 (2022); doi: https://doi.org/10.1101/2022.10.27.514007.

[87] F. A. Deeney and J. P. O'Leary, An experimental investigation of the process of isotope exchange that takes place when heavy water is exposed to the atmosphere, Eur. J. Phys. **30**, 871 (2009).

[88] 10.5291/ILL-DATA.EASY-1064 (D7).

[89] 10.5291/ILL-DATA.8-05-468 (IN12).

[90] 10.5286/ISIS.E.RB2220225-1 (LET).

[91] F. Mezei, Neutron spin echo: A new concept in polarized thermal neutron techniques, Z. Phys. A: Hadrons Nucl. **255**, 146 (1972).

[92] G. Cassella, J. R. Stewart, G. M. Paternò, V. G. Sakai, M. Devonport, P. J. Galsworthy, R. I. Bewley, D. J. Voneshen, D. Raspino, and G. J. Nilsen, Polarization analysis on the LET cold neutron spectrometer using a ^{3}He spin-filter: First results, J. Phys.: Conf. Ser. **1316**, 012007 (2019).

[93] G. L. Squires, *Introduction to the Theory of Thermal Neutron Scattering* (Cambridge University Press, Cambridge, UK, 2012).